2-1-2023

Neurobehavioral deficits of mice expressing a low level of G127V mutant frataxin.

Daniel Fil

Robbie L Conley

Aamir Zuberi

Cathleen Lutz

Terry Gemelli

See next page for additional authors

Authors

Daniel Fil, Robbie L Conley, Aamir Zuberi, Cathleen Lutz, Terry Gemelli, Marek Napierala, and Jill S Napierala

Neurobiology of Disease 177 (2023) 105996

Contents lists available at ScienceDirect

Neurobiology of Disease

journal homepage: www.elsevier.com/locate/ynbdi

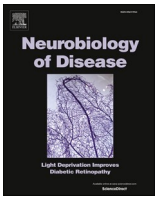

Neurobehavioral deficits of mice expressing a low level of G127V mutant frataxin

Daniel Fil [a,1,2], Robbie L. Conley [a,1], Aamir R. Zuberi [c], Cathleen M. Lutz [d], Terry Gemelli [b], Marek Napierala [a,3], Jill S. Napierala [a,*,3]

[a] Department of Biochemistry and Molecular Genetics, University of Alabama at Birmingham, Birmingham, AL 35294, USA
[b] Department of Neurology, Peter O'Donnell Jr. Brain Institute, University of Texas Southwestern Medical Center, Dallas, TX 75390, USA
[c] Technology Evaluation and Development, JAX Center for Precision Genetics, Rare Disease Translational Center, The Jackson Laboratory, Bar Harbor, ME 04609, USA
[d] The Rare and Orphan Disease Center, JAX Center for Precision Genetics, Rare Disease Translational Center, The Jackson Laboratory, Bar Harbor, ME 04609, USA

ARTICLE INFO

Keywords:
Frataxin
Friedreich's ataxia
Mitochondria
Point mutation

ABSTRACT

Friedreich's ataxia (FRDA) is a neurodegenerative disease caused by reduced expression of the mitochondrial protein frataxin (FXN). Most FRDA patients are homozygous for large expansions of GAA repeats in intron 1 of *FXN*, while some are compound heterozygotes with an expanded GAA tract in one allele and a missense or nonsense mutation in the other. A missense mutation, changing a glycine to valine at position 130 (G130V), is prevalent among the clinical variants. We and others have demonstrated that levels of mature FXN protein in FRDA G130V samples are reduced below those detected in samples harboring homozygous repeat expansions. Little is known regarding expression and function of endogenous FXN-G130V protein due to lack of reagents and models that can distinguish the mutant FXN protein from the wild-type FXN produced from the GAA-expanded allele. We aimed to determine the effect of the G130V (murine G127V) mutation on Fxn expression and to define its multi-system impact *in vivo*. We used CRISPR/Cas9 to introduce the G127V missense mutation in the Fxn coding sequence and generated homozygous mice ($Fxn^{G127V/G127V}$). We also introduced the G127V mutation into a GAA repeat expansion FRDA mouse model ($Fxn^{GAA230/KO}$; KIKO) to generate a compound heterozygous strain ($Fxn^{G127V/GAA230}$). We performed neurobehavioral tests on cohorts of WT and *Fxn* mutant animals at three-month intervals for one year, and collected tissue samples to analyze molecular changes during that time. The endogenous Fxn G127V protein is detected at much lower levels in all tissues analyzed from $Fxn^{G127V/G127V}$ mice compared to age and sex-matched WT mice without differences in *Fxn* transcript levels. $Fxn^{G127V/G127V}$ mice are significantly smaller than WT counterparts, but perform similarly in most neurobehavioral tasks. RNA sequencing analysis revealed reduced expression of genes in oxidative phosphorylation and protein synthesis, underscoring the metabolic consequences in our mouse model expressing extremely low levels of Fxn. Results of these studies provide insight into the unique pathogenic mechanism of the FXN G130V mechanism and the tolerable limit of Fxn/FXN expression *in vivo*.

1. Introduction

Friedreich's ataxia (FRDA) is a neurodegenerative disease where the vast majority (96%) of patients are homozygous for large expansions of GAA repeat sequences of intron 1 of the frataxin gene *FXN*. Some patients (4%) have a missense or nonsense mutation in one *FXN* allele and expanded GAAs in the other (compound heterozygotes) (Cossee et al., 1999; Durr and Brice, 1996; Filla et al., 1996; Galea et al., 2016). Several point mutations in the *FXN* coding region have been identified as pathogenic in a heterozygous state, with one mutation, FXN R165C, reported in a state of homozygosity (Candayan et al., 2020). The FXN G130V missense mutation is prevalent among individuals diagnosed with compound heterozygous FRDA, and is caused by a transversion mutation (c.389G > T) in the *FXN* coding sequence (Bidichandani et al.,

* Corresponding author.
E-mail address: Jill.Napierala@UTSouthwestern.edu (J.S. Napierala).
[1] Authors contributed equally to this work.
[2] Present address: Department of Biochemistry & Molecular Biology, University of Arkansas for Medical Sciences, Little Rock, AR 72205, USA.
[3] Present address: Department of Neurology, Peter O'Donnell Jr. Brain Institute, University of Texas Southwestern Medical Center, Dallas, TX 75390, USA.

https://doi.org/10.1016/j.nbd.2023.105996
Received 4 October 2022; Received in revised form 20 December 2022; Accepted 6 January 2023
Available online 10 January 2023

1997). FRDA patients with G130V mutations have been found to exhibit a milder clinical presentation and slower disease progression compared to FRDA patients with homozygous GAA repeat sequences (Bidichandani et al., 1997; Clark et al., 2017; Cossee et al., 1999; Forrest et al., 1998; McCabe et al., 2002), despite observed lower levels of mature FXN protein detected in peripheral tissues (Clark et al., 2017 Lazaropoulos et al., 2015 #6551). These patients have significantly lower incidences of cardiomyopathy, scoliosis and diabetes compared to FRDA patients with other FXN point mutations (Clark et al., 2017).

Complete loss of *Fxn* in mice causes peri-implantation lethality, as early as day 6.5 of embryonic development (E6.5), prior to gastrulation (Cossee et al., 2000). However, multiple mouse models have been generated to investigate pathogenicity of expanded GAA repeat tracts or various conditions of frataxin depletion *in vivo*, such as the GAA repeat expansion knock-in, *Fxn* knock out (KIKO; $Fxn^{GAA230/KO}$) model (Miranda et al., 2002); mice with homozygous deletion of *Fxn* carrying a human *FXN* transgene with an expanded GAA repeat (Pook et al., 2001; Anjomani Virmouni et al., 2015 #6472); neuronal and cardiac tissue-specific *Fxn* knock-out mice (Piguet et al., 2018; Puccio et al., 2001) and an inducible mouse model of *Fxn* deficiency generated by genomic integration of a *Fxn*-targeting shRNA transgene (Chandran et al., 2017). But animal models to study pathological conditions arising from expression of FXN point mutant proteins were not available until 2020. We generated and reported the first FRDA point mutation mouse model, Fxn G127V ($Fxn^{G127V/G127V}$), in order to define effects of this mutation (equivalent to the human pathogenic FXN G130V mutation) *in vivo* (Fil et al., 2020). More recently, a mouse model harboring the I151F (equivalent to FXN I154F) has been described (Medina-Carbonero et al., 2022). The $Fxn^{I151F/I151F}$ mice demonstrate low levels of Fxn and OXPHOS complex proteins along with reduced aconitase activity in brain and cardiac tissues compared to wild type (WT; $Fxn^{WT/WT}$) mice. Moreover, the molecular and biochemical alterations observed in $Fxn^{I151F/I151F}$ mice precede neurobehavioral deficits, such as reduced motor coordination, strength and locomotor activity (Medina-Carbonero et al., 2022).

Previously, we reported reduced perinatal survival of $Fxn^{G127V/G127V}$ mice and severe Fxn deficiency and mitochondrial aberrations in $Fxn^{G127V/G127V}$ murine embryonic fibroblasts (MEFs) (Fil et al., 2020). In the current study, we performed longitudinal neurobehavioral characterization and molecular analyses of our adult $Fxn^{G127V/G127V}$ mice. Our cohort included the well-characterized KIKO model ($Fxn^{GAA230/KO}$), reported to exhibit neurobehavioral phenotypes at nine months of age (McMackin et al., 2017; Pandolfo, 2014), and we crossed the $Fxn^{G127V/G127V}$ animals with $Fxn^{GAA230/KO}$ mice to generate compound heterozygous $Fxn^{G127V/GAA230}$ animals, resembling the pathological state of FRDA G130V patients.

Fxn protein expression is dramatically reduced in tissues from $Fxn^{G127V/G127V}$ mice compared to WT, despite unchanged transcript levels. We also found that the Fxn^{G127V} protein is soluble and localizes to mitochondria as seen with Fxn^{WT} protein. The $Fxn^{G127V/G127V}$ mice are small in size at birth and throughout life compared to their sex and age-matched counterparts and develop a hunched posture. The $Fxn^{G127V/G127V}$ mice also showed mild neurobehavioral deficits compared to WT, such as reduced velocity in open field tests, reduced grip strength and decreased stride length in gait analysis measurements. Finally, the presence of the *Fxn* allele with an expanded repeat (GAA230) did not aggravate any of the molecular or neurobehavioral phenotypes observed for the $Fxn^{G127V/G127V}$ mice. Hence, $Fxn^{G127V/G127V}$ mice survive into adulthood despite extremely low levels of Fxn and exhibit molecular and physical deficits that can be utilized as phenotypic readouts for FRDA therapeutic strategies, such as frataxin supplementation.

2. Materials and methods

2.1. Animals

Mice were bred and housed in the animal facility at the University of Alabama at Birmingham under 12 h light/dark conditions and fed *ad libitum*. Mice carrying the Fxn^{G127V} mutant allele were previously described (Fil et al., 2020). Breeders for the frataxin knock-in/knock-out (KIKO) strain were purchased from The Jackson Laboratory (stock #012329; B6.Cg-$Fxn^{tm1.1Pand}$ Fxn^{tm1Mkn}/J) and were bred with each other or were crossed with $Fxn^{G127V/WT}$ mice to generate the $Fxn^{GAA230/KO}$ and $Fxn^{G127V/GAA230}$ cohorts, respectively. All experimental procedures were conducted in accordance with Guide for the Care and Use of Laboratory Animals published by the National Institutes of Health (NIH Publication No. 85–23, revised 1996) and was approved by the Institutional Animal Care and Use Committee at University of Alabama at Birmingham.

2.2. Genotyping

Mouse genomic DNA was isolated from ~3mm tail biopsies with QuickExtract™ DNA Extraction Solution (Lucigen/Biosearch Tech QE09050) and served as a template for PCR reactions using JumpStart™ Taq ReadyMix™ (Sigma-Aldrich P2893) for amplification with allele-specific primers (Table S4). Genotyping of mice carrying the Fxn^{G127V} allele was performed by restriction fragment length polymorphism (RFLP) analysis as described (Fil et al., 2020).

Genotyping of $Fxn^{GAA230/KO}$ mice was conducted using allele-specific primer sequences provided by The Jackson Laboratory (Table S4). Cycling parameters were as follows: 2 min at 94 °C, followed by 32 cycles of 30 s at 94 °C, 30 s at 52 °C and 2 min at 72 °C, and finally 7 min at 72 °C. All genotyping reaction products were resolved by 1.5% agarose gel electrophoresis and visualized with ethidium bromide using a BioRad ChemiDoc MP Imaging system.

2.3. Neurobehavioral testing

Neurobehavioral testing began with four cohorts of 20 mice each (Table S1, 10 males and 10 females). Animals were scored at 3, 6, 9, and 12 month time points in the following order: open field, Catwalk, grip strength, hindlimb clasping, kyphosis.

2.4. Open field

General locomotor activity was analyzed using EthoVision XT video tracking software (Noldus). Mice were placed in the center of the Open Field arena, without prior training, and allowed to explore freely. The behavior was recorded for 10 min and aspects of their behavior, including total path traveled, average moving speed, frequency and duration of rapid movement (speed >100 mm/s), frequency and duration of immobility (speed <5 mm/s), were assessed. The arena was cleaned with chlorhexidine solution between animals.

2.5. Gait analysis

Detailed analysis of gait, individual paw placement and inter-limb coordination was performed using the Catwalk XT system (Noldus). Mice were placed on one side of a narrow, straight runway restricted by black plastic walls and allowed time to acclimate to the instrument until they voluntarily crossed the test area. Mouse paw placement was recorded as they walked from one side of the runway to the other until they completed three runs meeting the compliance parameters (run duration >0.5 s, max allowed variation in walking speed during the run <60%). The runway was cleaned with chlorhexidine solution between animals. Stride length and base of support for front and rear paws were assessed and the regularity index was calculated. Recorded data were

carefully analyzed for errors, such as non-paw signals (*e.g.* tail, nose, *etc.*), and manually classified for each run (Chen et al., 2017).

2.6. Grip strength

Assessment of neuromuscular function was performed by recording the peak amount of force an animal exerted in grasping a grip placed at their forelimb. The Grip Strength meter (Chatillon DFE) was positioned horizontally and the mice were held by the tail and lowered toward the grip strength platform. The animal was allowed to grasp the forelimb grip and was pulled backwards in the horizontal plane until it lost its grip. The measurement was repeated 4–5 times and the maximum force applied to the grip was recorded.

2.7. Kyphosis

Dorsal curvature of the spine was assessed as described (Guyenet, 2010). Briefly, mice were removed from the cage, placed on a flat surface and observed as they walked. Kyphosis score 0–3 was assigned based on the following criteria: 0 - no kyphosis, mouse can easily straighten its spine as it walks; 1 - mild kyphosis when stationary, the animal can straighten its spine as it walks; 2 - unable to straighten its spine completely and maintains persistent but mild kyphosis; 3 - pronounced kyphosis as it walks or while stationary.

2.8. Hindlimb clasping

Corticospinal function was assessed by scoring limb clasping as described (Guyenet, 2010). Briefly, mice were lifted by the base of the tail and hindlimb position observed for 10 s. A clasping score from 0 to 3 was assigned based on the following criteria: 0- no clasping, hindlimbs are consistently splayed outward; 1- one hindlimb is retracted toward the abdomen for >50% of the time suspended; 2- both hindlimbs are partially retracted toward the abdomen for >50% of the time suspended; 3- hindlimbs are entirely retracted and touching the abdomen for >50% of the time suspended.

2.9. Body weight analysis

Mouse body weights were recorded once a week from 1 to 12 months of age using an electronic balance (Ohaus CX221).

2.10. Quantification of mRNA by RT-qPCR and RNA sequencing

RNA was isolated from fresh or flash frozen tissues by RNeasy Mini Kit (Qiagen 74104). Contaminating genomic DNA was removed with TURBO DNA-free™ Kit (Invitrogen AM1907). The level of specific mRNA was quantitated by Power SYBR™ Green RNA-to-CT™ 1-Step Kit (Applied Biosystems 4389986). *Fxn* transcript levels relative to that of a housekeeping gene, glyceraldehyde phosphate dehydrogenase (*Gapdh*) or hypoxanthine phosphoribosyltransferase 1 (*Hprt*), were calculated using the ΔΔCt method, as described (Fil et al., 2020). Primer sequences are given in Table S4.

Next-generation RNA sequencing (RNA-seq) experimental groups included three animals per genotype (two males and one female, except for $Fxn^{G127V/GAA230}$, which had one male and two females). A total amount of 1 μg RNA per cerebral cortex sample was used as input material for RNA sample preparations for RNA-seq. Sequencing libraries were generated using NEBNext® Ultra TM RNA Library Prep Kit for Illumina® (New England Biolabs) following the manufacturer's recommendations and index codes were added to attribute sequences to each sample. Briefly, mRNA was purified from total RNA using poly-T oligo-attached magnetic beads. Fragmentation was carried out using divalent cations under elevated temperature in NEBNext® First Strand Synthesis Reaction Buffer (5×). First strand cDNA was synthesized using random hexamer primers and M-MuLV Reverse Transcriptase. Second strand cDNA synthesis was subsequently performed using DNA Polymerase I and RNase H. In order to select cDNA fragments of preferentially 250–300 base pairs (bp) in length, the library fragments were purified with the AMPure XP system (Beckman Coulter, Beverly, USA). Library quality was assessed on an Agilent Bioanalyzer 2100 system. The NovaSeq 6000 PE150 (Illumina) platform was used to generate paired-end 150 bp reads. Paired-end clean reads were aligned to the reference mouse genome (GRCm38/mm10) using the Spliced Transcripts Alignment to a Reference (STAR) software. FeatureCounts was used to count the read numbers mapped to each gene. Differential expression analysis between the groups was performed using DESeq2. Downstream analyses were conducted using Partek Flow, String (Szklarczyk et al., 2021) and ShinyGO (Ge et al., 2020; Kanehisa et al., 2021).

2.11. Western blot

Flash frozen tissues collected at different timepoints (Table S2) were processed for protein lysates. Tissues were homogenized in lysis buffer (0.1% NP-40, 0.25 M NaCl, 5 mM EDTA, 50 mM Hepes, pH 7.5) supplemented with 1% protease inhibitor cocktail (PIC, Sigma P8340), and centrifuged at 20,000 xg for 10 min. Supernatants were collected and protein concentrations were determined by Bradford assay using Protein Assay Dye Reagent (Bio-Rad 5000006). Lysates were heated with reducing sample buffer (50 mM Tris, pH 6.8, 2% SDS, 0.1% bromophenol blue, 10% glycerol, 100 mM DTT) for 3 min at 95 °C, and were resolved on 4–12% NuPAGE gels and transferred to nitrocellulose membranes. Membranes were blocked with 5% milk in Tris-buffered saline with Tween-20 (TBST; 10 mM Tris-HCl, pH 7.5, 150 mM NaCl, 0.1% Tween-20) followed by incubation with primary antibody (anti-FXN, Proteintech 14147–1-AP; anti-HPRT, Proteintech 15059–1-AP; anti-Aconitase, Cell Signaling 6922; anti-Gapdh, Millipore MAB374) and secondary antibody (anti-Rabbit HRP linked, GE Healthcare NA934V or anti-Mouse HRP linked, GE Healthcare NA931V). Finally, SuperSignal™ West Femto (Thermo Fisher 34094) or SuperSignal™ West Dura Extended Duration Substrate (Thermo Fisher 34075) was used for chemiluminescent detection.

Mitochondria enriched protein lysates were prepared as described (Lin et al., 2017), with modifications. Isolated fresh brain hemispheres were briefly homogenized in hypotonic buffer [225 mM mannitol, 75 mM sucrose, 5 mM Hepes, 1 mM EGTA, 0.1 mM EDTA (pH 8), 0.1% BSA, 1% PIC, kept on ice for 10 min, then homogenized extensively. The suspensions were centrifuged at 1500 rcf, 4 min, 4 °C, after which supernatants were transferred to fresh tubes and re-centrifuged at 20,000 rcf, 15 min, 4 °C. Supernatants were collected as "cytoplasmic" fractions and pellets were washed with buffer [50 mM Tris (pH 7.5), 0.25 M sucrose, 0.2 mM EDTA (pH 8), 0.1% BSA, 1% PIC], then resuspended in lysis buffer [0.1% NP40, 0.25 M NaCl, 5 mM EDTA, 50 mM Hepes (pH 7.5), 1% PIC] and kept on ice for 10 min for protein extraction. Lysates were centrifuged at 20,000 rcf, 10 min, 4 °C and clarified supernatants were transferred to fresh tubes as "mitochondria enriched" fractions.

2.12. Statistical analyses

Statistical analyses were conducted using GraphPad Prism 8 or 9. For neurobehavioral studies involving assessments of cohorts at multiple timepoints (body weight, velocity, grip strength, stride length, base of support, regularity index), Ordinary two-way ANOVA with Dunnett's multiple comparisons tests were performed with $Fxn^{WT/WT}$ as the control comparison. For molecular analyses involving multiple groups (RT-qPCR and western blots), Ordinary one-way ANOVA with Dunnett's multiple comparisons tests were performed with $Fxn^{WT/WT}$ as the control comparison. For comparison of two groups, unpaired, two-tailed Student's *t*-tests were performed. For all tests, differences were considered significant for comparisons in which $p < 0.05$.

3. Results

3.1. Gross phenotypic characteristics of mice carrying Fxn^{G127V} mutant alleles

We generated mice carrying G127V mutant alleles (Fxn^{G127V}), equivalent to the human G130V clinical variant observed in FRDA patients (Fil et al., 2020). Sequencing of cDNA prepared from cerebral cortex of $Fxn^{G127V/WT}$ mice confirmed expression of full-length, uninterrupted Fxn^{G127V} transcripts and Fxn^{WT} transcripts in these mice (Fig. S1). Crossing $Fxn^{G127V/WT}$ mice with the established FRDA GAA repeat expansion knock-in, knock-out model (KIKO) (Miranda et al., 2002), allowed us to generate a *Fxn* compound heterozygous model ($Fxn^{G127V/GAA230}$) resembling the genetic context of FRDA G130V patients. We generated cohorts of $Fxn^{WT/WT}$, $Fxn^{G127V/G127V}$, $Fxn^{G127V/GAA230}$ and $Fxn^{GAA230/KO}$ mice to be tested in neurobehavioral tasks (Table S1) and to be sacrificed for molecular analyses (Table S2). Weights of animals in our neurobehavioral cohort were recorded weekly for one year and results clearly demonstrate that $Fxn^{G127V/G127V}$ animals are significantly smaller than mice of any other genotype compared at any point during the timecourse, beginning at 12 weeks of age (Fig. 1A, B). Representative photographs of $Fxn^{WT/WT}$ and $Fxn^{G127V/G127V}$ mice (males and females) of approximately one year of age qualitatively show the persistent size discrepancy (Fig. 1C). $Fxn^{G127V/WT}$ mice are of similar

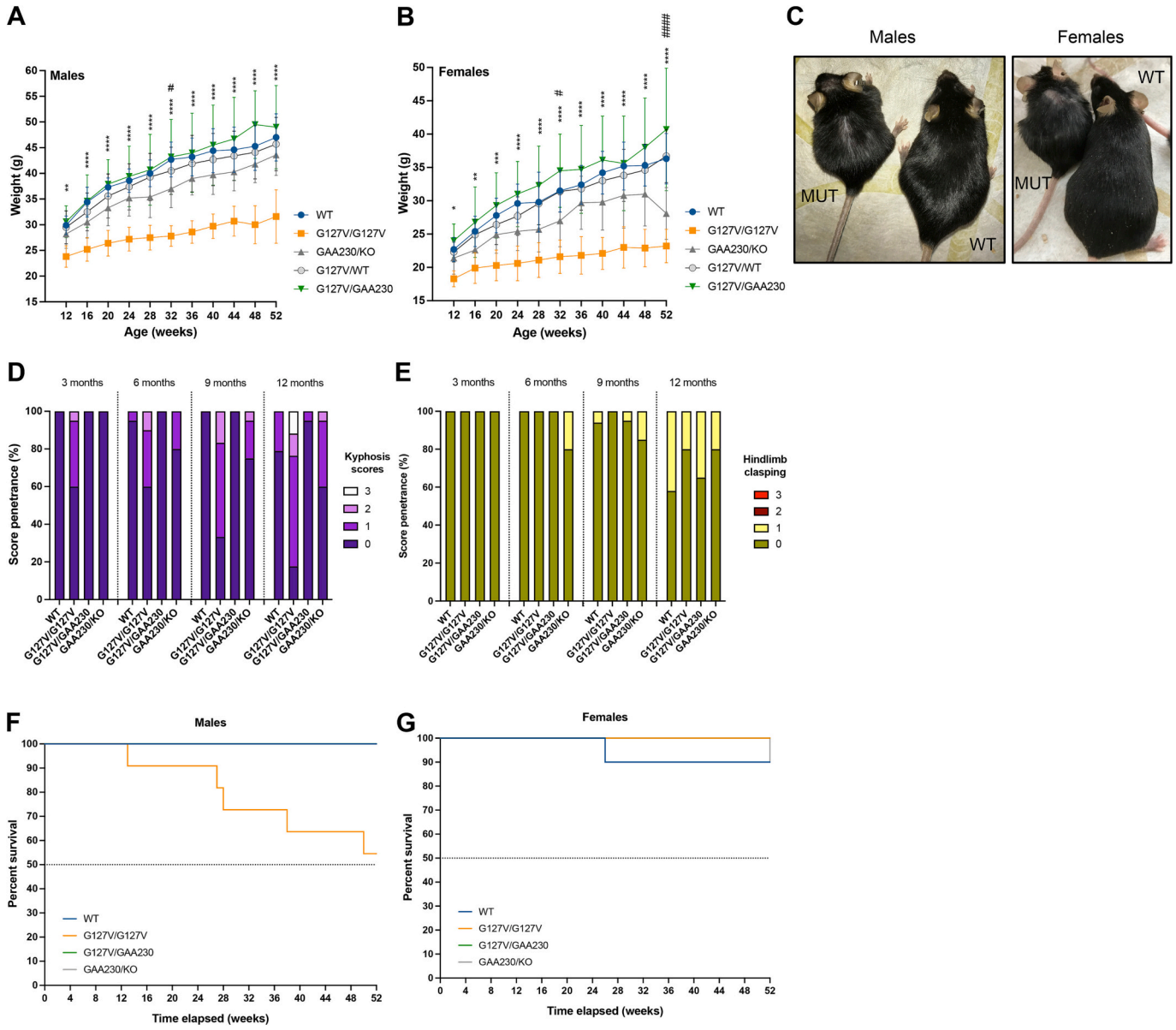

Fig. 1. $Fxn^{G127V/G127V}$ mice are small in size, develop a hunched posture and males show reduced survival. (A, B) Mice were weighed weekly and the average weight of mice in each group ($n = 10$ males/group, 10 = females/group) is plotted at four week intervals for males (A) and females (B) beginning at 12 weeks of age. Error bars represent standard deviation (SD) and significant differences are denoted as: * $p < 0.05$, ** $p < 0.01$, *** $p < 0.001$, **** $p < 0.0001$ for comparisons between $Fxn^{G127V/G127V}$ and $Fxn^{WT/WT}$ mice and # $p < 0.05$ for comparisons between $Fxn^{GAA230/KO}$ and $Fxn^{WT/WT}$ mice. (C) Photographs of representative $Fxn^{WT/WT}$ and $Fxn^{G127V/G127V}$ mice at approximately one year of age (females - left, males – right). (D) Mice from each group (Table S1) were scored for presence of kyphosis at 3, 6, 9 and 12 months of age. A score was recorded for each mouse and presented as percent penetrance for each genotype at the indicated timepoint. (E) Mice from each group (Table S1) were scored for presence of hindlimb clasping at 3, 6, 9 and 12 months of age. A score was recorded for each mouse and presented as a percent penetrance for each genotype at the indicated timepoint. (F, G) Kaplan-Meier curves were created for male (F) and female (G) mice for each group. Results are shown as percent survival for each genotype.

weight to $Fxn^{WT/WT}$ mice (Fig. 1A, B), indicating that the Fxn^{G127V} allele is not acting as a dominant negative to drive the low body weight phenotype.

In addition to their observed small body weight and size, $Fxn^{G127V/G127V}$ mice develop a mild curvature of the spine (kyphosis), akin to scoliosis, as early as three months of age. The phenotype becomes more severe and penetrant by 12 months of age (Fig. 1D). Of note, $Fxn^{GAA230/KO}$ mice in our cohort also developed mild to moderate kyphosis as they aged. A hallmark feature denoting progression of certain cerebellar ataxias in mouse models is hindlimb clasping, whereby an animal involuntarily retracts one or both of its hindlimbs toward its abdomen when suspended by its tail (Guyenet, 2010). This phenotype was not consistently observed for $Fxn^{G127V/G127V}$ mice, however, 20% of $Fxn^{G127V/GAA230}$ animals demonstrated mild (score of 1) but persistent clasping after 6 months of age (Fig. 1E). At 12 months of age, mice from each genotype demonstrated slight clasping, suggesting that age rather than genotype influenced the presentation. Finally, over the course of one year, we recorded deaths of five $Fxn^{G127V/G127V}$ male mice (50% of the cohort) and one $Fxn^{WT/WT}$ female mouse (10% of the cohort) (Fig. 1F, G and Table S1).

3.2. The G127V mutation reduces Fxn protein levels at the post-transcriptional level

Fxn transcript levels were measured by real-time RT-qPCR using a primer pair spanning *Fxn* exons 4 and 5 in cerebral cortex, cerebellum, spinal cord and heart samples isolated from three month old mice. Significantly reduced levels of *Fxn* mRNA were observed only in tissue samples prepared from $Fxn^{GAA230/KO}$ mice, showing a 40–50% reduction compared to $Fxn^{WT/WT}$ samples (Fig. 2 A-D). On the other hand, western blot analysis of whole tissue lysates prepared from three month old mice revealed significantly reduced Fxn protein levels in $Fxn^{G127V/G127V}$, $Fxn^{G127V/GAA230}$ and $Fxn^{GAA230/KO}$ cerebral cortex, cerebellum, spinal cord and heart samples compared to those from $Fxn^{WT/WT}$ animals (Fig. 3), with the same patterns observed at the 12 month timepoint (Fig. S2). Notably, Fxn protein levels were reduced to 30–40% in $Fxn^{G127V/GAA230}$ and $Fxn^{GAA230/KO}$ samples compared to $Fxn^{WT/WT}$, while they were at or below the limit of detection in $Fxn^{G127V/G127V}$ whole tissue lysates.

We previously determined that the Fxn G127V protein localizes to mitochondria in $Fxn^{G127V/G127V}$ MEFs (Fil et al., 2020). Therefore, to increase the probability of detecting Fxn G127V in the tissue samples from the homozygous model, brain homogenates were enriched for mitochondria prior to western blot analysis. Fxn G127V was detected in soluble mitochondria lysate, albeit at greatly reduced levels compared to Fxn WT protein, but was not detected in cytosolic or insoluble mitochondria fractions (Fig. 4A). Quantification of Fxn G127V signal in $Fxn^{G127V/G127V}$ mitochondria-enriched lysates revealed levels reduced to 1.7% relative to the Fxn WT protein signal quantified in $Fxn^{WT/WT}$ lysates (Fig. 4B).

3.3. $Fxn^{G127V/G127V}$ mice exhibit strength and endurance deficits

Cohorts of FRDA mouse models ($Fxn^{G127V/G127V}$, $Fxn^{G127V/GAA230}$ and $Fxn^{GAA230/KO}$) were tested alongside $Fxn^{WT/WT}$ mice at 3, 6, 9 and 12 months of age to assess free locomotor activity (open field), strength (forelimb grip strength) and gait (Catwalk). At three months of age, $Fxn^{G127V/G127V}$ male mice showed significantly reduced distance traveled and velocity, as shown by representative recorded traces from open field testing (Fig. 5A) and quantitatively (Fig. 5B). However, velocity of

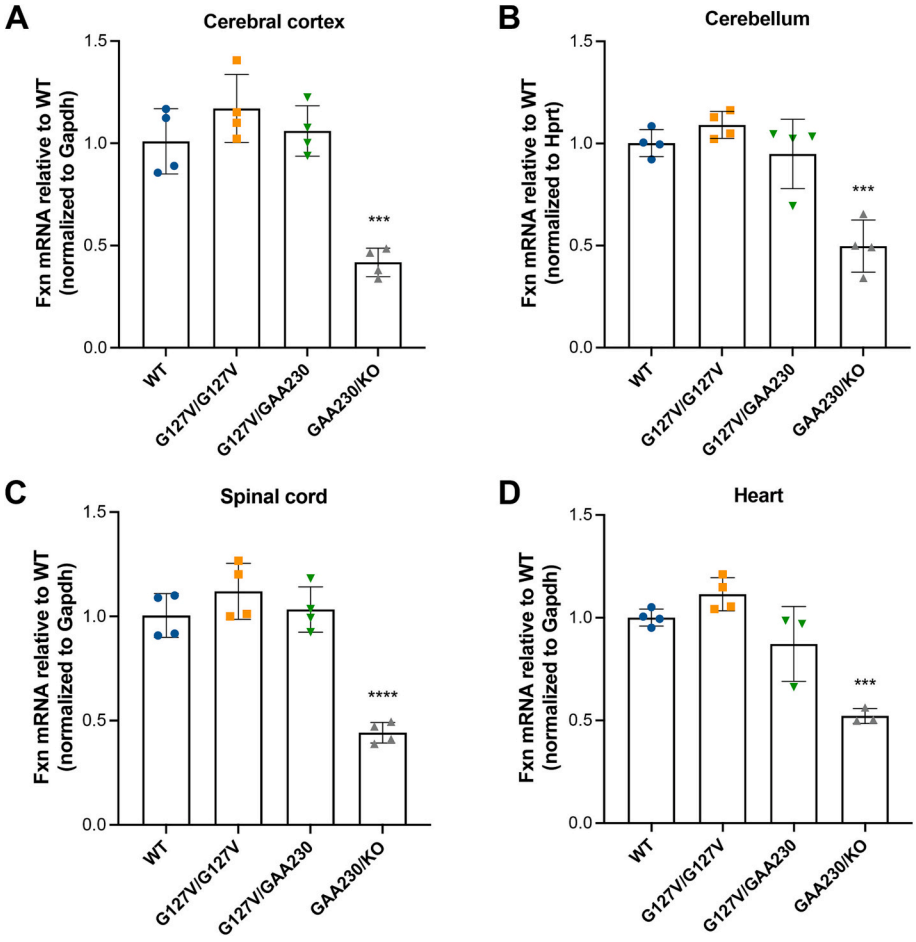

Fig. 2. The G127V mutation does not impact expression of the *Fxn* transcript in tissues of G127V knock-in models. Real-time RT-qPCR analysis of Fxn mRNA in total RNA prepared from (A) cerebral cortex (B) cerebellum (C) spinal cord or (D) heart tissue homogenates from 3 month old mice. *Fxn* transcript levels were normalized to *Gapdh* or *Hprt* and are plotted relative to $Fxn^{WT/WT}$ samples. Bars represent mean ± SD ($n = 4$/group) and significant differences are denoted by asterisks (* $p < 0.05$, *** $p < 0.001$, **** $p < 0.0001$).

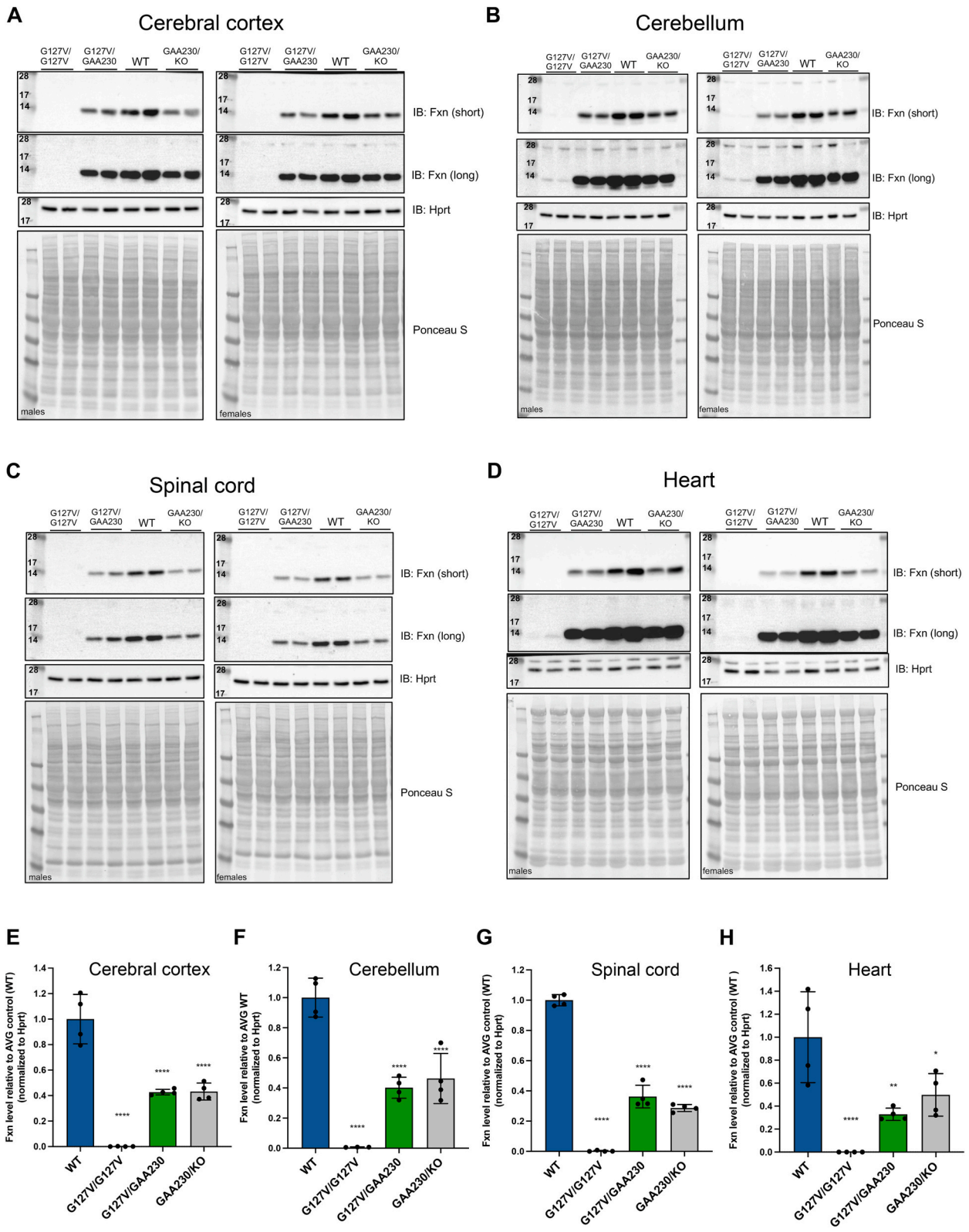

Fig. 3. Fxn protein expression is dramatically reduced in tissues of $Fxn^{G127V/G127V}$ mice. Western blot analysis of Fxn in (A) cerebral cortex (B) cerebellum (C) spinal cord (D) heart homogenates prepared from $Fxn^{G127V/G127V}$, $Fxn^{G127V/GAA230}$, $Fxn^{GAA230/KO}$ and $Fxn^{WT/WT}$ mice. The blots represent immunodetectable Fxn from lysates prepared from two male (left panel) and two female (right panel) three-month old mice per group. Two different exposure times are shown for Fxn bands – short (30 s; top panel) and long (5 min; lower panel). Hprt signal and Ponceau S staining serve as loading controls. Molecular weights are provided (kDa) in the first lane of each blot. (E - H) Quantification of Fxn signal (short exposure) from blots shown in (A-D) respectively, normalized to Hprt and plotted relative to $Fxn^{WT/WT}$ samples. Bars represent mean ± SD (n = 4/group) and significant differences are denoted by asterisks (* $p < 0.05$, ** $p < 0.01$, **** $p < 0.0001$). Abbreviations: IB (immunoblot).

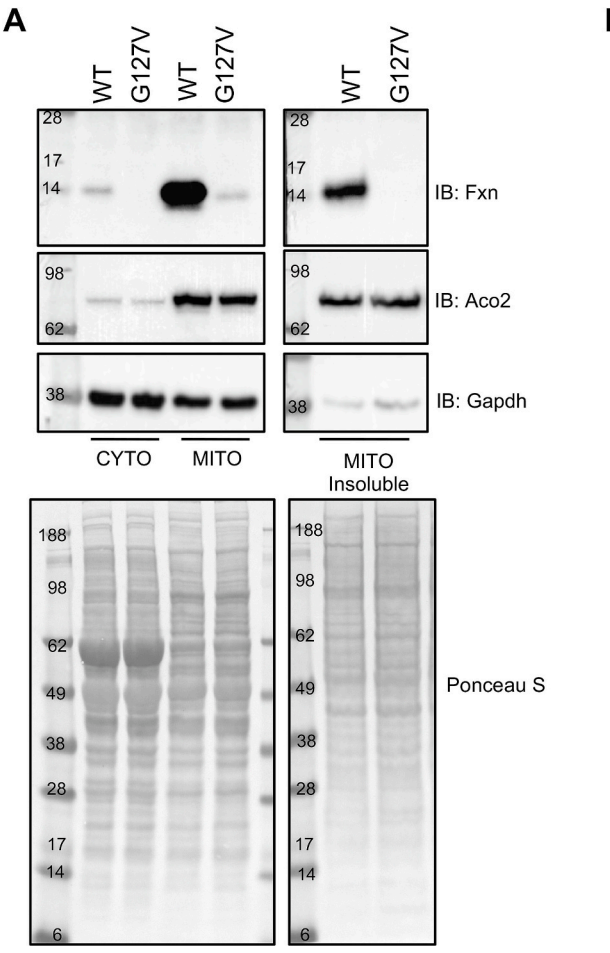

Fig. 4. Fxn G127V protein is soluble and localizes to mitochondria. (A) Representative western blot analysis of subcellular fractions prepared from brain homogenates (one hemisphere per sample) of $Fxn^{G127V/G127V}$ and $Fxn^{WT/WT}$ aged to 12 months. Aconitase (Aco2) expression serves as a positive control for integrity of the mitochondria fraction and Gapdh as a marker of the cytosolic fraction. (B) Quantification of western blot analyses of Fxn G127V protein detected in soluble mitochondrial fractions, as shown in (A). Bars represent mean ± SD (n = 4 samples/group) and a significant difference is denoted by asterisks (**** $p < 0.0001$). Abbreviations: IB (immunoblot).

movement for $Fxn^{G127V/G127V}$ males remained steady as they aged while velocities decreased for the other male mice tested (Fig. 5B). The exception is when the mice were tested at 12 months of age, $Fxn^{G127V/G127V}$ males moved faster and more than males from any other group (Fig. 5B, C). $Fxn^{G127V/G127V}$ females, on the other hand, showed reduced velocity while moving during open field testing compared to the other female FRDA mouse models and $Fxn^{WT/WT}$ mice at 3 months of age, with significantly decreased speed recorded at all later timepoints (Fig. 5D, E). Moreover, at all timepoints tested, the $Fxn^{G127V/G127V}$ females spent significantly less time moving during the timed open field tests (Fig. 5F).

Forelimb grip strength steadily declined with age for both males and females for each genotype analyzed, as expected, with significantly reduced strength noted for $Fxn^{G127V/G127V}$ males compared to $Fxn^{WT/WT}$ males at 6 and 9 months of age and for $Fxn^{G127V/G127V}$ females compared to $Fxn^{WT/WT}$ females at 6 months of age (Fig. 6A, B).

Several dynamic gait parameters were measured using the Catwalk XT system (Noldus), an automated tool to collect quantitative locomotor data (Batka et al., 2014; Chen et al., 2017; Kyriakou et al., 2016; Walter et al., 2020). Stride length is a measure of the distance between the successive placement of the same paw (Walter et al., 2020). Each paw was recorded separately, then right and left paws were averaged for the hindlimbs and forelimbs. We found that stride length for the hindlimbs was significantly shorter for $Fxn^{G127V/G127V}$ males at 3 and 6 months of age compared to age-matched $Fxn^{WT/WT}$ males and the stride measured for forelimbs was significantly shorter for $Fxn^{G127V/G127V}$ males at 3 and 6 months of age (Figs. 6C and S3A). Hindlimb stride length was also significantly reduced at 6 and 12 months of age for $Fxn^{G127V/GAA230}$ male mice compared to $Fxn^{WT/WT}$ males, while front limb stride length was significantly reduced at 9 months (Figs. 6C and S3A). No differences in stride length (hind or front) were observed between $Fxn^{WT/WT}$ and $Fxn^{GAA230/KO}$ male mice. Female $Fxn^{G127V/G127V}$ mice showed significantly decreased hindlimb stride length compared to $Fxn^{WT/WT}$ females at all ages except 9 months, and at 6 and 12 months for stride length of the front limbs (Figs. 6D and S3B). Interestingly, $Fxn^{GAA230/KO}$ females demonstrated increased hind and forelimb stride lengths compared to $Fxn^{WT/WT}$ females at 6 months of age and $Fxn^{G127V/GAA230}$ females had significantly longer front limb stride lengths compared to $Fxn^{WT/WT}$ females at 3 months of age (Figs. 6D and S3B).

Base of support was a separate gait parameter recorded in our analysis that was exclusively and significantly reduced in $Fxn^{G127V/G127V}$ compared to $Fxn^{WT/WT}$ mice at 6 and 9 months of age (males) for the hindlimbs (Fig. 6E) and 3 months of age (females) for forelimbs (Fig. S3D). Taken together, these results indicate subtle gait anomalies for $Fxn^{G127V/G127V}$ mice, although these particular parameters (stride length and base of support) could be influenced by the reduced body size of $Fxn^{G127V/G127V}$ mice (Fig. 1A, B).

Finally, we measured interpaw coordination by analyzing the normal step sequence patterns (NSSPs) for every mouse. The results are plotted as a regularity index (%), which conveys the number of NSSPs recorded over the total number of times the paws are placed (Baldwin et al., 2017; Batka et al., 2014; Vrinten and Hamers, 2003). The regularity index as a percentage is independent of the combination or number of the six NSSP classifications used in a run. A value of 100% indicates no deviation from use of NSSPs, while anything below indicates an irregular walking pattern. With a few exceptions, mice (males and females) of all genotypes displayed normal walking patterns (>90% regularity index) at all ages analyzed (Fig. 6G, H), indicating that *Fxn* mutations (G127V or GAA230) did not impact interlimb coordination of the animals analyzed

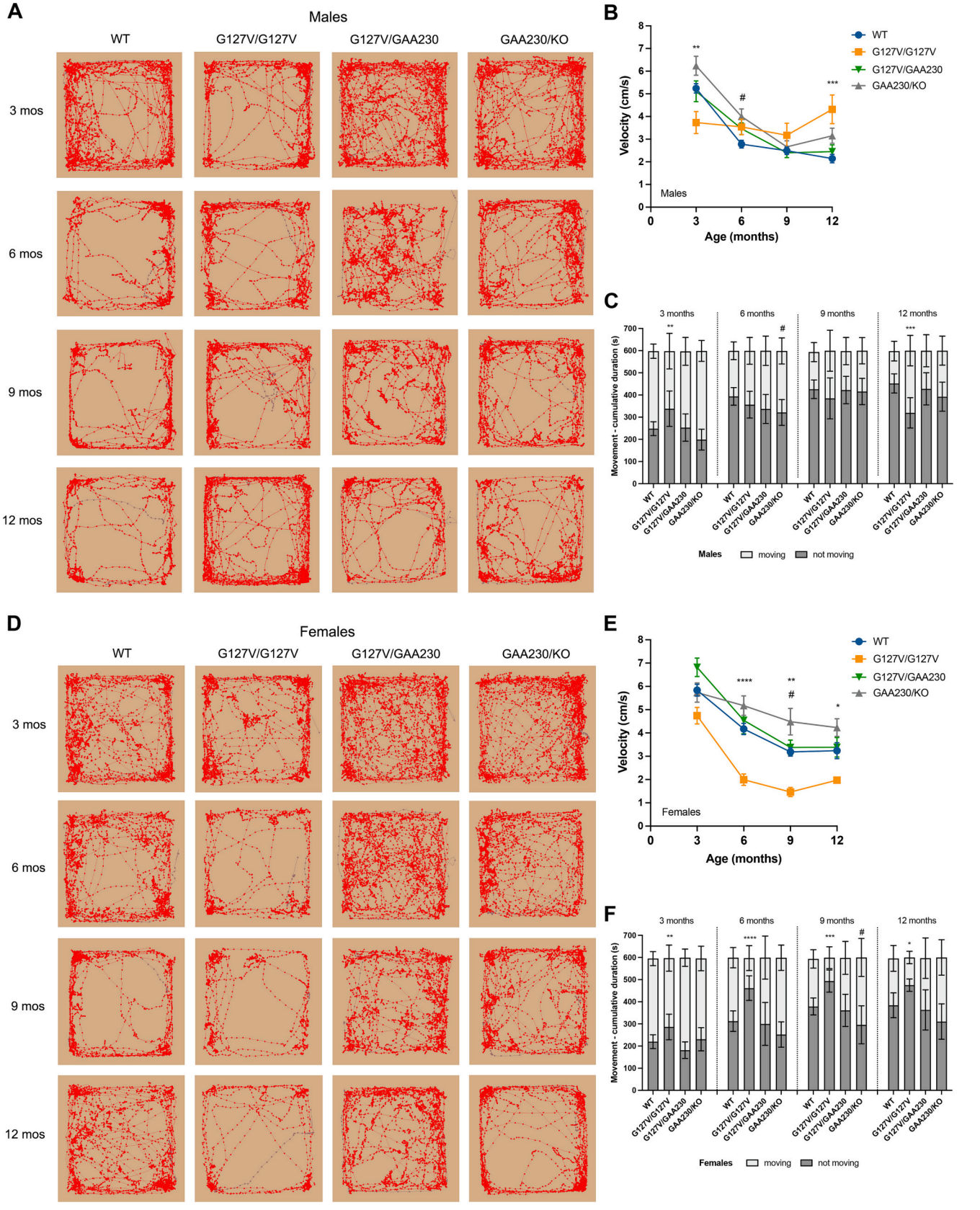

(caption on next page)

Fig. 5. Female $Fxn^{G127V/G127V}$ mice show reduced locomotor activity. (A) Representative traces obtained from open field activity tests performed on male mice of indicated groups (top) at 3, 6, 9 and 12 months of age. Free movement was recorded and is indicated by red lines. (B) Quantification of velocity measurements obtained during open field tests. Velocity (cm/s) was calculated as total distance traveled (cm) over test duration ($t = 600$ s) and plotted as the mean value ± SD per genotype at each timepoint tested. Significant differences are denoted as ** $p < 0.01$, *** $p < 0.001$ for comparisons between $Fxn^{G127V/G127V}$ and $Fxn^{WT/WT}$ mice and # $p < 0.05$ for comparisons between $Fxn^{GAA230/KO}$ and $Fxn^{WT/WT}$ mice. (C) Cumulative duration of movement was quantified for each animal and is plotted as seconds spent "moving" or "not moving" during open field testing. Bars represent mean ± SD for each category and significant differences are denoted as ** $p < 0.01$, *** $p < 0.001$ for comparisons between $Fxn^{G127V/G127V}$ and $Fxn^{WT/WT}$ mice and # $p < 0.05$ for comparisons between $Fxn^{GAA230/KO}$ and $Fxn^{WT/WT}$ mice. (D, E, F) Data and analysis for experiments performed on female mice exactly as described for males in (A, B, C). Significant differences are denoted as * $p < 0.05$, ** $p < 0.01$, *** $p < 0.001$, **** $p < 0.0001$ for comparisons between $Fxn^{G127V/G127V}$ and $Fxn^{WT/WT}$ mice and # $p < 0.05$ for comparisons between $Fxn^{GAA230/KO}$ and $Fxn^{WT/WT}$ mice. (For interpretation of the references to colour in this figure legend, the reader is referred to the web version of this article.)

in our study cohort.

3.4. Downregulation of genes involved in oxidative phosphorylation and protein synthesis pathways in $Fxn^{G127V/G127V}$ mice

To evaluate the effect of Fxn G127V mutation on gene expression, we conducted transcriptome analysis of $Fxn^{G127V/G127V}$, $Fxn^{G127V/GAA230}$ and $Fxn^{GAA230/KO}$ in comparison to $Fxn^{WT/WT}$ mice. Total RNA from cerebral cortices isolated from three animals in each group was subjected to RNA-seq. Principal component analysis of the data demonstrated that presence of $Fxn^{G127V/G127V}$ allele, either in a homozygous state or in combination with Fxn^{GAA230} allele, elicits a substantially different transcriptome than $Fxn^{WT/WT}$ or $Fxn^{GAA230/KO}$ animals (Fig. 7A). Lists of differentially expressed (DE) transcripts obtained by pairwise comparison between each group can be found in Table S3. We focused our analyses predominantly on differences between $Fxn^{G127V/G127V}$ and $Fxn^{WT/WT}$ samples. A total of 426 transcripts were DE in $Fxn^{G127V/G127V}$ when compared to $Fxn^{WT/WT}$ cerebral cortex samples (FDR ≤ 0.005, Table S3). STRING functional association network analysis separated these DE transcript groups into three major clusters overlapping with the top three KEGG pathways distinguishing $Fxn^{G127V/G127V}$ from $Fxn^{WT/WT}$ animals: oxidative phosphorylation (blue), ribosomes (red) and proteasome (green) (Fig. 7B, C). Other KEGG pathways shown as affected by the Fxn G127V point mutation are listed in Fig. 7C. Our analyses of the RNA-seq data identified 426 DE transcripts between $Fxn^{WT/WT}$ and $Fxn^{G127V/G127V}$ animals and 754 DE transcripts between $Fxn^{WT/WT}$ and $Fxn^{G127V/GAA230}$ mice (at FDR < 0.005) (Fig. S4A). Comparison of these two FRDA mouse models revealed only 44 commonly DE transcripts. KEGG pathways analysis of these 44 DE transcripts identified oxidative phosphorylation as the most significantly over-represented pathway (Fig. S4B). Oxidative phosphorylation, ribosome and proteasome were the most significantly affected pathways in the 426 DE transcripts between $Fxn^{WT/WT}$ and $Fxn^{G127V/G127V}$ animals (Fig. 7C). Similar pathways were also identified in the group of 382 genes uniquely dysregulated in $Fxn^{G127V/G127V}$ when compared to $Fxn^{WT/WT}$ (Fig. S4C). However, 710 genes that were uniquely dysregulated in $Fxn^{G127V/GAA230}$ animals when compared to $Fxn^{WT/WT}$ were enriched in pathways related to addiction, synapses and signaling (Fig. S4D). A direct comparison between $Fxn^{G127V/G127V}$ and $Fxn^{G127V/GAA230}$ identified 884 DE transcripts enriched in ribosome, oxidative phosphorylation as well as synapses, signaling and addiction – a combination of the pathways dysregulated in both animal models when compared to $Fxn^{WT/WT}$ (Fig. S4E). Further examination of gene expression patterns in the oxidative phosphorylation and ribosome pathways clearly demonstrated that nearly all DE genes are significantly downregulated in $Fxn^{G127V/G127V}$ mice (Fig. 7D), indicating a severe metabolic imbalance caused by the Fxn G127V missense mutation at the cellular level.

4. Discussion

Friedreich's ataxia is a severe multisystem disorder with a typical onset in childhood or adolescence and relentless progression over subsequent decades of adult life. The relatively slow progression of the disease causes numerous challenges in conducting clinical trials but also presents with difficulties in establishing animal models with phenotypes robust enough that could be utilized in preclinical studies.

In higher organisms, frataxin is required to sustain life and its complete knockout in mouse is early embryonic lethal (Cossee et al., 2000). Numerous FRDA mouse models created thus far can be categorized into two groups: (i) mouse frataxin deficiency from the earliest developmental stages; This group includes all GAA expansion animals (humanized transgenic and mouse knock-in) and Fxn point mutation models (I151F (Medina-Carbonero et al., 2022) and G127V described herein); (ii) animals in which Fxn depletion is induced at a certain stage of development and decreases rapidly from levels characteristic for wild-type animals to null or nearly null; These mice are represented by inducible knockdown and conditional knock-out mice (Chandran et al., 2017; Piguet et al., 2018; Puccio et al., 2001). The critical distinction between these two groups is severity of the phenotype. Rapid decrease of Fxn does not recapitulate the natural progression of FRDA, but results in onset of severe phenotypes and frequently a significantly shortened lifespan. On the other hand, a decreased amount of Fxn (or FXN) from birth resembles, at the cellular level, the FXN downregulation observed in FRDA patients. However, these models present with significantly milder phenotypic changes, frequently detected only by performing extensive and thorough behavioral analyses with large animal cohorts.

This is also the case in $Fxn^{G127V/G127V}$ mice described herein. Homozygous animals are significantly smaller, frequently demonstrate a hunched back posture, move less and have reduced grip strength. Half of the males in our $Fxn^{G127V/G127V}$ cohort died prior to the study endpoint of 12 months (Table S1). However, this early mortality phenomenon is not observed for $Fxn^{G127V/G127V}$ males kept in our main colony, suggesting that the premature deaths were associated with stress of repeated handling or neurobehavioral testing. Life spans of $Fxn^{G127V/G127V}$ females, or mice of other groups included in the 12 month study, were not impacted despite being housed and analyzed under identical conditions, suggesting that the environment (housing) was not causative.

The relatively mild movement phenotypes observed are in stark contrast with extremely low frataxin protein levels detected in cells and tissues from these mice ((Fil et al., 2020) and Figs. 3, 4, S2). Using multiple antibodies, recognizing different epitopes and different mouse tissues, we determined that $Fxn^{G127V/G127V}$ mice express approximately 1% of the amount of protein found in $Fxn^{WT/WT}$ mice. Surprisingly, this minimal amount of Fxn is sufficient for animal development. $Fxn^{G127V/G127V}$ mice present with a distinct pathological phenotype (perinatal mortality (Fil et al., 2020), small body size, hunched posture), but only mild alterations to strength and locomotor function. Similar to $Fxn^{G127V/G127V}$, a second reported FRDA point mutation mouse model I151F, presents with a very low level of frataxin (below 6%) and relatively modest phenotypic and molecular changes when compared to the $Fxn^{WT/WT}$ animals (Medina-Carbonero et al., 2022).

On the other hand, RNA-seq analyses revealed quite dramatic transcriptome aberrations with significant downregulation of mRNAs encoding proteins involved in critical oxidative phosphorylation and ribosome pathways. In fact, out of 426 DE transcripts between $Fxn^{G127V/G127V}$ and $Fxn^{WT/WT}$, only 26 (6%) were upregulated in $Fxn^{G127V/G127V}$ cerebral cortex while the remaining 400 (94%) were downregulated. This strongly indicates a global metabolic change caused by low

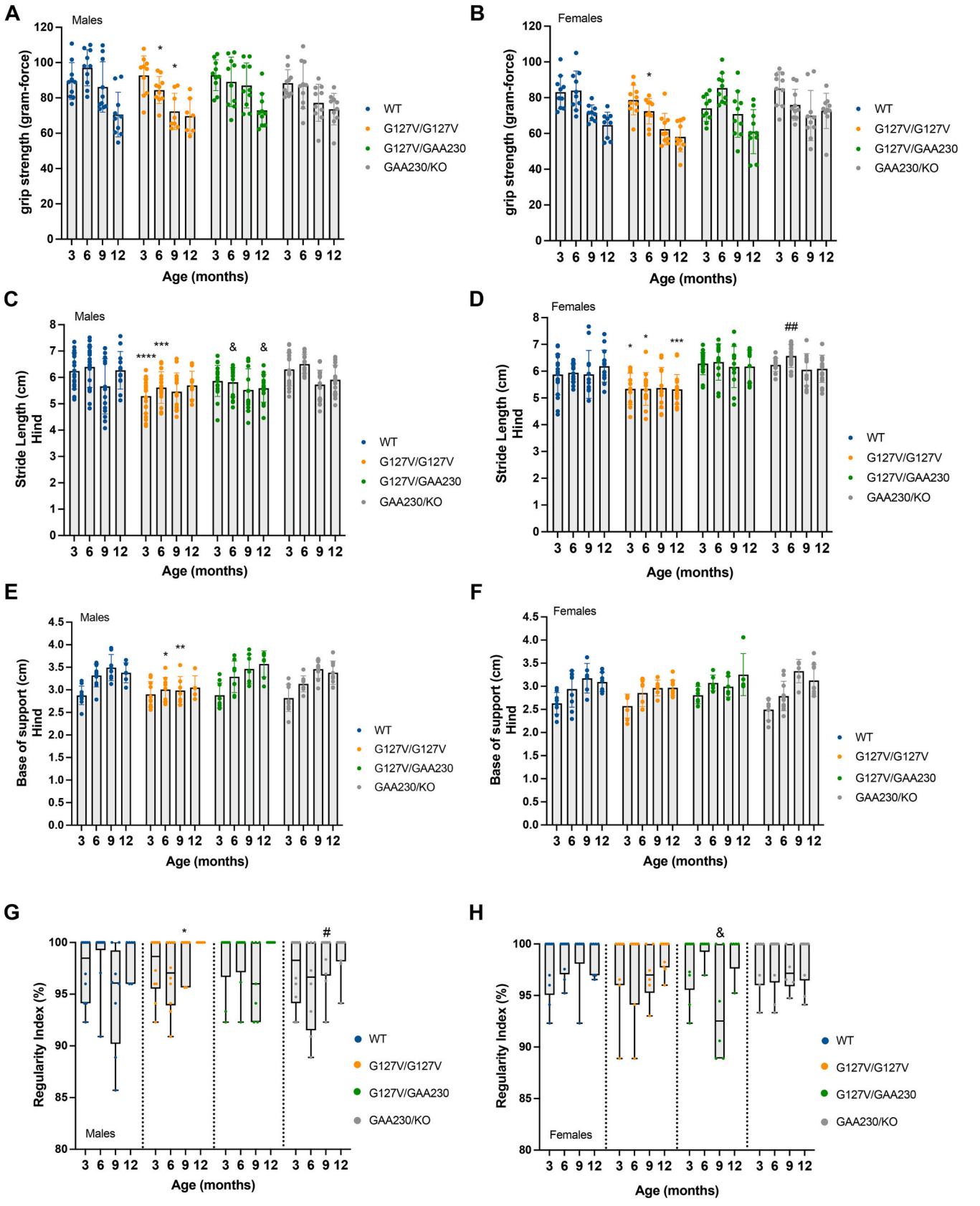

(caption on next page)

Fig. 6. *Fxn*$^{G127V/G127V}$ mice have reduced strength and subtle gait abnormalities. (A) Analysis of forelimb strength was conducted on *Fxn*$^{G127V/G127V}$, *Fxn*$^{G127V/GAA230}$, *Fxn*$^{GAA230/KO}$ and *Fxn*$^{WT/WT}$ mice at 3, 6, 9 and 12 months. Bars represent mean ± SD and significant differences are denoted as * $p < 0.05$ for comparisons between *Fxn*$^{G127V/G127V}$ and *Fxn*$^{WT/WT}$ mice. (B) Grip strength results for female mice as described for males in (A). (C) Hindlimb stride length was recorded for male mice of each group at 3, 6, 9 and 12 months of age. Bars represent mean ± SD and significant differences are denoted as *** $p < 0.001$, **** $p < 0.0001$ for comparisons between *Fxn*$^{G127V/G127V}$ and *Fxn*$^{WT/WT}$ mice, and & $p < 0.05$ for comparisons between *Fxn*$^{G127V/GAA230}$ and *Fxn*$^{WT/WT}$ mice. (D) Results of stride length analysis for female mice as described for males in (C). Significant differences are denoted as * $p < 0.05$, *** $p < 0.001$ for comparisons between *Fxn*$^{G127V/G127V}$ and *Fxn*$^{WT/WT}$ mice and ## $p < 0.01$ for comparison between *Fxn*$^{GAA230/KO}$ and *Fxn*$^{WT/WT}$ mice. (E) Base of support was measured for male mice of each group at 3, 6, 9 and 12 months of age. Bars represent mean ± SD and significant differences are denoted as * $p < 0.05$, ** $p < 0.01$ for comparisons between *Fxn*$^{G127V/G127V}$ and *Fxn*$^{WT/WT}$ mice. (F) Results of base of support analysis for female mice as described for males in (E). (G) Regularity index of step sequence was calculated and reported as a percentage of deviation from the use of normal step sequence patterns, with 100% indicating no deviation from normal. Bars represent mean ± SD and significant differences are denoted as * $p < 0.05$ for comparisons between *Fxn*$^{G127V/G127V}$ and *Fxn*$^{WT/WT}$ mice, # $p < 0.05$ for comparisons between *Fxn*$^{GAA230/KO}$ and *Fxn*$^{WT/WT}$ mice and & $p < 0.05$ for comparisons between *Fxn*$^{G127V/GAA230}$ and *Fxn*$^{WT/WT}$ mice.

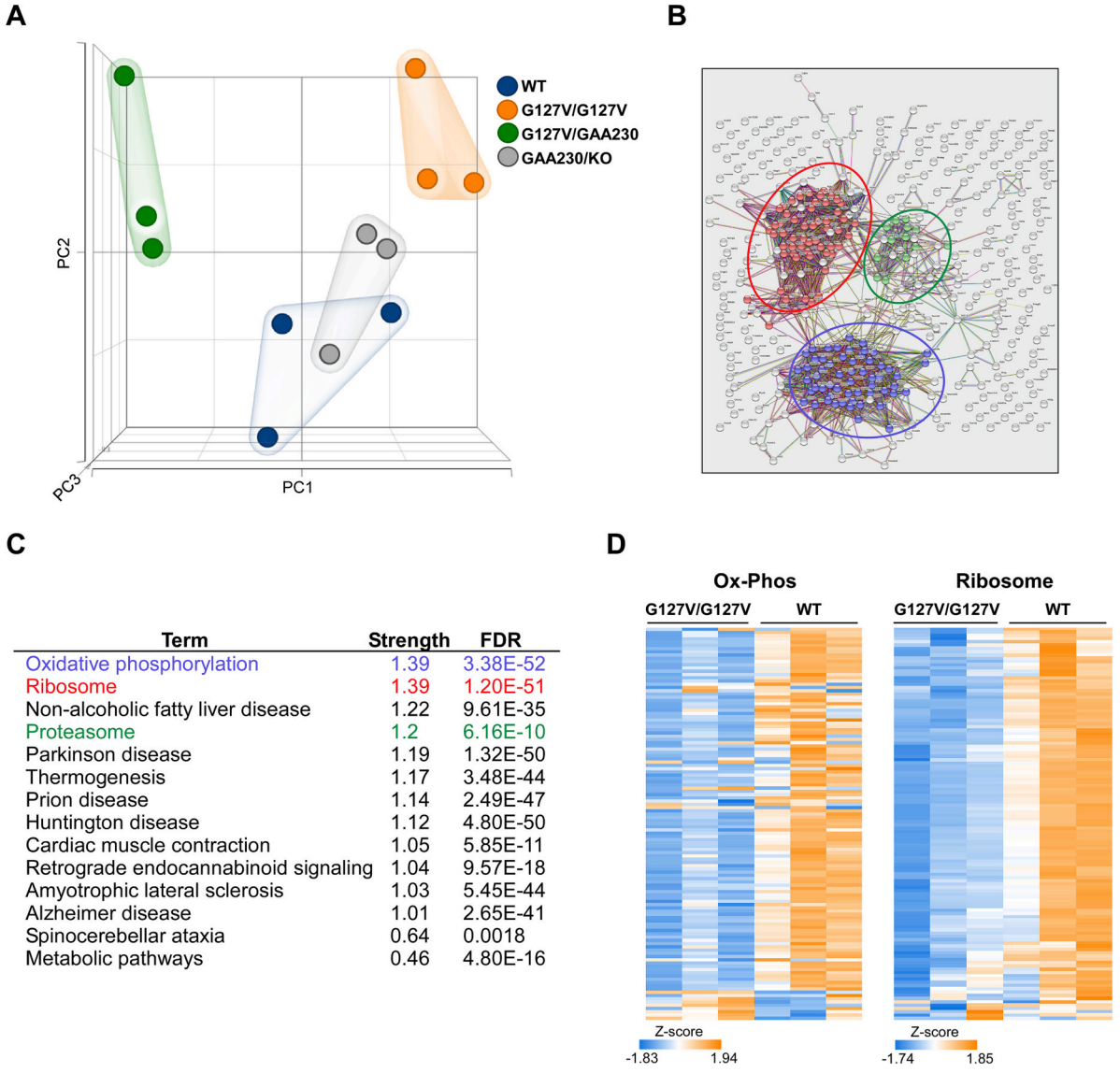

Term	Strength	FDR
Oxidative phosphorylation	1.39	3.38E-52
Ribosome	1.39	1.20E-51
Non-alcoholic fatty liver disease	1.22	9.61E-35
Proteasome	1.2	6.16E-10
Parkinson disease	1.19	1.32E-50
Thermogenesis	1.17	3.48E-44
Prion disease	1.14	2.49E-47
Huntington disease	1.12	4.80E-50
Cardiac muscle contraction	1.05	5.85E-11
Retrograde endocannabinoid signaling	1.04	9.57E-18
Amyotrophic lateral sclerosis	1.03	5.45E-44
Alzheimer disease	1.01	2.65E-41
Spinocerebellar ataxia	0.64	0.0018
Metabolic pathways	0.46	4.80E-16

Fig. 7. Analysis of RNA-seq data obtained from cerebral cortex samples of *Fxn*$^{G127V/G127V}$ mice. Cohorts of three animals per each genotype were used in the studies. (A) Principle component analysis of the RNA-seq data demonstrating clear separation between transcriptome profiles of mice expressing at least one Fxn G127V allele (*Fxn*$^{G127V/G127V}$ - orange, *Fxn*$^{G127V/GAA230}$ – green) and the remaining genotypes (*Fxn*$^{WT/WT}$ – blue, *Fxn*$^{GAA230/KO}$ – gray). (B) Functional protein association network analysis using STRING. The 426 transcripts differentially expressed between *Fxn*$^{G127V/G127V}$ and *Fxn*$^{WT/WT}$ animals served as the input for the analyses. Circled are three major clusters corresponding to KEGG pathways: oxidative phosphorylation (indicated in blue), ribosome (indicated in red) and proteasome (indicated in green). (C) List of major KEGG pathways dysregulated in cerebral cortex of *Fxn*$^{G127V/G127V}$ compared to *Fxn*$^{WT/WT}$ mice. FDR indicates significance of the enrichment. (D) Heatmap illustrating expression of 121 genes in the oxidative phosphorylation pathway (KEGG mmu00190) and 120 genes included in the ribosome pathway (KEGG mmu03010). (For interpretation of the references to color in this figure legend, the reader is referred to the web version of this article.)

expression of mutant Fxn G127V, resulting in downregulation of numerous processes to adjust to the conditions imposed by such a severe frataxin deficit.

These findings also indicate that mice can tolerate significantly lower levels of frataxin than human cells. On average, FRDA cells express 10–30% of frataxin found in an unaffected, non-carrier population (Deutsch et al., 2010; Lazaropoulos et al., 2015; Napierala et al., 2017; Napierala et al., 2021). Results obtained from $Fxn^{G127V/G127V}$ mouse studies may also explain why animals carrying expanded GAA repeats exhibit subtle, not-fully penetrant phenotypic changes (Al-Mahdawi et al., 2006; Anjomani Virmouni et al., 2015; Gerard et al., 2022; McMackin et al., 2017; Miranda et al., 2002). As shown in this and numerous prior studies, both humanized transgenic and GAA knock-in mice express levels of frataxin exceeding 10% of the amount present in $Fxn^{WT/WT}$ mice (Al-Mahdawi et al., 2006; Anjomani Virmouni et al., 2015; Gerard et al., 2022; Lin et al., 2017; Miranda et al., 2002; Pook et al., 2001), at least an order of magnitude more than found in $Fxn^{G127V/G127V}$ animals.

In FRDA patients, clinical consequences of frataxin depletion are not noticeable at birth, but typically manifest after a few years of life. Likely, an interplay of both progressive accumulation of mitochondrial/cellular lesions caused by frataxin insufficiency and adaptation/compensation of the nervous system determine disease onset. Perhaps lack of a severe ataxia phenotype in $Fxn^{G127V/G127V}$ mice, despite extremely low frataxin levels, results from the short animal lifespan, efficient compensatory mechanisms employed by rodents or differences in physiology between humans and rodents. By the same rationale, conditional Fxn KO or shRNA Fxn mice demonstrate robust phenotypic changes due to such a rapid decrease of Fxn levels, too fast for implementation of any compensatory mechanisms.

Our studies defined a minimum amount frataxin required for mouse development. While we were able to obtain $Fxn^{G127V/G127V}$ mice (expressing approximately 1% of frataxin relative to $Fxn^{WT/WT}$), we were unsuccessful in generating $Fxn^{G127V/KO}$ animals that would express approximately 50% of the frataxin detected in $Fxn^{G127V/G127V}$ mice. From the perspective of disease modeling, conclusions arising from these experiments are rather discouraging: there appears to be a very narrow window for the level of Fxn that is compatible with life that is also sufficient to sustain relatively normal functions of the animals. Thus, generating FRDA mouse models with robust phenotypes based on inherited Fxn depletion will likely be very challenging.

However, we cannot discuss $Fxn^{G127V/G127V}$ mouse model purely in the context of the dramatically reduced frataxin level. Fxn G127V is a mutated frataxin protein and in humans, FRDA G130V compound heterozygote patients present with distinct and rather milder symptoms (Bidichandani et al., 1997; Caron et al., 2015; Cossee et al., 1999; Galea et al., 2016; McCabe et al., 2002). The G130V mutation affects both maturation and thermodynamic stability of FXN (Cavadini et al., 2000; Clark et al., 2017; Correia et al., 2008), however the effect of this point mutation on frataxin functions is unclear. We cannot exclude the possibility that FXN G130V (and Fxn G127V) carries out distinct functions or performs its activity with different kinetics, thus affecting clinical presentations or phenotypes. It is interesting to speculate that FXN G130V (Fxn G127V) is a less stable but functionally "better" frataxin that can more efficiently compensate the overall frataxin deficit in FRDA G130V patients, which is also a dramatic loss compared to homozygous repeat expansion patients (Clark et al., 2017; Doni et al., 2021; Lazaropoulos et al., 2015), and $Fxn^{G127V/G127V}$ animals, thus allowing the mice to survive expressing a very low amount of frataxin.

To summarize, the $Fxn^{G127V/G127V}$ mouse model fills an important gap in FRDA animal models between phenotypically mild GAA repeat expansion models and severely impaired mice caused by rapid and drastic depletion of Fxn observed in shRNA or in conditional Fxn knockout FRDA models. It represents a model of severe and inherited frataxin decrease that displays moderate and traceable phenotypes. These characteristics make the $Fxn^{G127V/G127V}$ mouse a good model to study consequences of frataxin deficiency and a tool for development of therapeutic approaches, especially those relying on frataxin replacement or supplementation.

Funding

This work was supported by Friedreich's Ataxia Research Alliance (General Research Grant to J.S.N.), National Institutes of Health National Institute of Neurological Disorders and Stroke (R03NS099953 to J.S.N., R01NS121038 to M.N.).

Authorship contributions

Conceptualization: A.Z., C.L., J.S.N. and M.N. Data curation and Investigation: D.F., A.Z., R.C., T.G. and J.S.N. Formal analysis: D.F., A.Z., R.C., C.L., T.G., J.S.N. and M.N. Funding acquisition: J.S.N. and M.N. Writing - original draft: J.S.N. and M.N. Writing - review and editing: D. F., R.C., A.Z., C.L., T.G., J.S.N., M.N.

Declaration of Competing Interest

The authors report no competing interests.

Data availability

Data will be made available on request.

Acknowledgments

The authors wish to thank all members of the Napierala laboratory for critical comments and helpful discussions throughout the project and acknowledge the UAB Neuroscience Behavioral Assessment Core for providing access to key equipment for the study.

Appendix A. Supplementary data

Supplementary data to this article can be found online at https://doi.org/10.1016/j.nbd.2023.105996.

References

Al-Mahdawi, S., et al., 2006. GAA repeat expansion mutation mouse models of Friedreich ataxia exhibit oxidative stress leading to progressive neuronal and cardiac pathology. Genomics. 88, 580–590.
Anjomani Virmouni, S., et al., 2015. A novel GAA-repeat-expansion-based mouse model of Friedreich's ataxia. Dis. Model. Mech. 8, 225–235.
Baldwin, H.A., et al., 2017. Step sequence is a critical gait parameter of unilateral 6-OHDA Parkinson's rat models. Cell Transplant. 26, 659–667.
Batka, R.J., et al., 2014. The need for speed in rodent locomotion analyses. Anat Rec (Hoboken). 297, 1839–1864.
Bidichandani, S.I., et al., 1997. Atypical Friedreich ataxia caused by compound heterozygosity for a novel missense mutation and the GAA triplet-repeat expansion [letter]. Am. J. Hum. Genet. 60, 1251–1256.
Candayan, A., et al., 2020. The first biallelic missense mutation in the FXN gene in a consanguineous Turkish family with Charcot-Marie-tooth-like phenotype. Neurogenetics. 21, 73–78.
Caron, E., et al., 2015. Atypical presentation for Friedreich Ataxia in a child. J. Clin. Neuromuscul. Dis. 17, 13–17.
Cavadini, P., et al., 2000. Human frataxin maintains mitochondrial iron homeostasis in Saccharomyces cerevisiae. Hum. Mol. Genet. 9, 2523–2530.
Chandran, V., et al., 2017. Inducible and reversible phenotypes in a novel mouse model of Friedreich's Ataxia. Elife. 6.
Chen, H., et al., 2017. Establishing a reliable gait evaluation method for rodent studies. J. Neurosci. Methods 283, 92–100.
Clark, E., et al., 2017. Selected missense mutations impair frataxin processing in Friedreich ataxia. Ann Clin Transl Neurol. 4, 575–584.
Correia, A.R., et al., 2008. Dynamics, stability and iron-binding activity of frataxin clinical mutants. FEBS J. 275, 3680–3690.
Cossee, M., et al., 1999. Friedreich's ataxia: point mutations and clinical presentation of compound heterozygotes. Ann. Neurol. 45, 200–206.
Cossee, M., et al., 2000. Inactivation of the Friedreich ataxia mouse gene leads to early embryonic lethality without iron accumulation. Hum. Mol. Genet. 9, 1219–1226.

Deutsch, E.C., et al., 2010. A rapid, noninvasive immunoassay for frataxin: utility in assessment of Friedreich ataxia. Mol. Genet. Metab. 101, 238–245.
Doni, D., et al., 2021. The displacement of frataxin from the mitochondrial cristae correlates with abnormal respiratory supercomplexes formation and bioenergetic defects in cells of Friedreich ataxia patients. FASEB J. 35, e21362.
Durr, A., Brice, A., 1996. Genetics of movement disorders. Curr. Opin. Neurol. 9, 290–297.
Fil, D., et al., 2020. Mitochondrial damage and senescence phenotype of cells derived from a novel frataxin G127V point mutation mouse model of Friedreich's ataxia. Dis. Model. Mech. 13.
Filla, A., et al., 1996. The relationship between trinucleotide (GAA) repeat length and clinical features in Friedreich ataxia. Am. J. Hum. Genet. 59, 554–560.
Forrest, S.M., et al., 1998. The correlation of clinical phenotype in Friedreich ataxia with the site of point mutations in the FRDA gene. Neurogenetics. 1, 253–257.
Galea, C.A., et al., 2016. Compound heterozygous FXN mutations and clinical outcome in friedreich ataxia. Ann. Neurol. 79, 485–495.
Ge, S.X., et al., 2020. ShinyGO: a graphical gene-set enrichment tool for animals and plants. Bioinformatics. 36, 2628–2629.
Gerard, C., et al., 2022. A promising mouse model for Friedreich Ataxia progressing like human patients. Behav. Brain Res. 436, 114107.
Guyenet, S.J., et al., 2010. A simple composite phenotype scoring system for evaluating mouse models of cerebellar ataxia. J. Vis. Exp. 21 (39), 1787. https://doi.org/10.3791/1787.
Kanehisa, M., et al., 2021. KEGG: integrating viruses and cellular organisms. Nucleic Acids Res. 49, D545–D551.
Kyriakou, E.I., et al., 2016. Automated quantitative analysis to assess motor function in different rat models of impaired coordination and ataxia. J. Neurosci. Methods 268, 171–181.
Lazaropoulos, M., et al., 2015. Frataxin levels in peripheral tissue in Friedreich ataxia. Ann Clin Transl Neurol. 2, 831–842.
Lin, H., et al., 2017. Early cerebellar deficits in mitochondrial biogenesis and respiratory chain complexes in the KIKO mouse model of Friedreich ataxia. Dis. Model. Mech. 10, 1343–1352.
McCabe, D.J., et al., 2002. Intrafamilial phenotypic variability in Friedreich ataxia associated with a G130V mutation in the FRDA gene. Arch. Neurol. 59, 296–300.
McMackin, M.Z., et al., 2017. Neurobehavioral deficits in the KIKO mouse model of Friedreich's ataxia. Behav. Brain Res. 316, 183–188.
Medina-Carbonero, M., et al., 2022. Mice harboring the FXN I151F pathological point mutation present decreased frataxin levels, a Friedreich ataxia-like phenotype, and mitochondrial alterations. Cell. Mol. Life Sci. 79, 74.
Miranda, C.J., et al., 2002. Frataxin knockin mouse. FEBS Lett. 512, 291–297.
Napierala, J.S., et al., 2017. Comprehensive analysis of gene expression patterns in Friedreich's ataxia fibroblasts by RNA sequencing reveals altered levels of protein synthesis factors and solute carriers. Dis. Model. Mech. 10, 1353–1369.
Napierala, J.S., et al., 2021. Reverse phase protein Array reveals correlation of retinoic acid metabolism with cardiomyopathy in Friedreich's Ataxia. Mol. Cell. Proteomics 20, 100094.
Pandolfo, M., 2014. Movement Disorders. Elsevier, Inc, Genetics and Models.
Piguet, F., et al., 2018. Rapid and complete reversal of sensory Ataxia by gene therapy in a novel model of Friedreich Ataxia. Mol. Ther. 26, 1940–1952.
Pook, M.A., et al., 2001. Rescue of the Friedreich's ataxia knockout mouse by human YAC transgenesis. Neurogenetics. 3, 185–193.
Puccio, H., et al., 2001. Mouse models for Friedreich ataxia exhibit cardiomyopathy, sensory nerve defect and Fe-S enzyme deficiency followed by intramitochondrial iron deposits. Nat. Genet. 27, 181–186.
Szklarczyk, D., et al., 2021. The STRING database in 2021: customizable protein-protein networks, and functional characterization of user-uploaded gene/measurement sets. Nucleic Acids Res. 49, D605–D612.
Vrinten, D.H., Hamers, F.F., 2003. 'CatWalk' automated quantitative gait analysis as a novel method to assess mechanical allodynia in the rat; a comparison with von Frey testing. Pain. 102, 203–209.
Walter, J., et al., 2020. The CatWalk XT(R) is a valid tool for objective assessment of motor function in the acute phase after controlled cortical impact in mice. Behav. Brain Res. 392, 112680.